EPJ manuscript No.
(will be inserted by the editor)

Electron capture and ionization cross-section calculations for proton collisions with methane and the DNA and RNA nucleobases

Hans Jürgen Lüdde[1], Marko Horbatsch[2], and Tom Kirchner[2]

[1] Frankfurt Institute for Advanced Studies (FIAS), D-60438 Frankfurt, Germany
[2] Department of Physics and Astronomy, York University, Toronto, Ontario M3J 1P3, Canada

Received: date / Revised version: date

Abstract. Net ionization and net capture cross-section calculations are presented for proton collisions with methane molecules and the DNA/RNA nucleobases adenine, cytosine, guanine, thymine, and uracil. We use the recently introduced independent-atom-model pixel counting method to calculate these cross sections in the 10 keV to 10 MeV impact energy range and compare them with results obtained from the simpler additivity rule, a previously used complete-neglect-of-differential-overlap method, and with experimental data and previous calculations where available. It is found that all theoretical results agree reasonably well at high energies, but deviate significantly in the low-to-intermediate energy range. In particular, the pixel counting method which takes the geometrical overlap of atomic cross sections into account is the only calculation that is able to describe the measurements for capture in proton-methane collisions down to 10 keV impact energy. For the nucleobases it also yields a significantly smaller cross section in this region than the other models. New measurements are urgently required to test this prediction.

PACS. 34.10.+x General theories and models of atomic and molecular collisions and interactions – 34.50.Gb Electronic excitation and ionization of molecules – 34.70.+e Charge transfer

1 Introduction

Collisions involving biomolecules and DNA/RNA building blocks in particular have received an increasing amount of attention in recent years, largely because of their relevance in applications such as radiation protection and hadron therapy (see, e.g., Refs. [1,2] and references therein). In the context of the latter it is a well-established fact that most of the damage done to biological tissue stems from low-energy electrons (and to a lesser extent from free radicals) which are produced as secondary particles in ion-impact collisions and attack DNA/RNA molecules in direct ionization and dissociative electron attachment processes (and in chemical reactions). [3,4]. Cross-section information on both primary and secondary processes contributes to the understanding of the radiation damage problem, e.g., by providing input for Monte-Carlo simulations of particle tracks in biological matter [5] and by informing multiscale models which link microscopic processes on the electronic level with macroscopic biological effects on the cellular level [6,7].

Collisions involving complex molecules pose a significant challenge to theory owing to their large number of degrees of freedom and their multi-center geometry. While a few first-principles calculations have been reported in recent years [8,9,10,11], most of the available cross-section information is based on simplified approaches. A convenient framework for such a simplified discussion is offered by the independent atom model (IAM) according to which certain properties and quantities of a molecule are *constitutive*, i.e., can be obtained by adding up atomic contributions. When applied to collisions, the simplest version of the IAM consists in adding up the cross sections of the atomic constituents of a given molecule in order to obtain the molecular cross section. This procedure is usually referred to as the additivity rule (AR). It goes back to Bragg [12] and was first studied in a more systematic fashion in the 1950s for electron-impact ionization of medium-sized molecules [13]. The IAM-AR has since been applied to many electron- and ion-impact collision systems, typically with good success at high impact energies, while larger discrepancies with experimental data have been found in the low-to-intermediate energy region. This has been taken as an indication that molecular structure effects gain importance with decreasing collision energy [14].

Accordingly, extensions and alternatives have been considered, such as ARs with weight factors (see, e.g., [15] and the review article [16] and references therein) and a complete-neglect-of-differential-overlap (CNDO) approach (see, e.g., [14,17,18]). The latter starts from the assumption that a molecular net cross section can be expressed as a sum of partial cross sections for all initially occupied

molecular orbitals (MOs) and then approximates those partial cross sections as linear combinations of atomic-orbital (AO) specific cross sections with weight factors that are obtained from a Mulliken population analysis [19]. In this way, the CNDO approach takes molecular structure information into account to some extent. However, CNDO cross sections do not depend on the orientation of the molecule relative to the projectile beam direction, i.e., they are to be interpreted as orientation-averaged quantities. The same is, of course, true for the simple IAM-AR. Moreover, none of these methods account for the rotational-vibrational motion of the molecule, but this is uncritical for the impact energy ranges considered.

We have recently introduced an amended AR with orientation-dependent weight factors [20,21]. The weights are obtained from a geometrical interpretation of a molecular cross section as an effective area made up of overlapping atomic cross sections. The atomic cross sections are calculated using a first-principles-based method with ground-state density-functional-theory (DFT) potentials [22], and the effective area encountered by the impinging projectile is computed using a pixel counting method (PCM). The latter step is repeated for a large number of orientations so that the orientation average can be compared with experimental data for randomly oriented molecules. We refer to this model as IAM-PCM [21].

Previous applications of the IAM-PCM to proton collisions with medium-sized molecules such as H_2O and from larger compounds such as water clusters and a variety of biomolecules have shown promising results [20,21,23]. At high impact energies where the simple IAM-AR works well, the overlap effects are small and the IAM-PCM cross sections agree with the IAM-AR results. Toward lower energies they deviate and tend to be in better agreement with the (scarce) experimental data, i.e., our results suggest that the IAM-PCM represents an improvement compared to the IAM-AR.

The purpose of the present work is to further establish the IAM-PCM as a viable tool for net ionization and capture cross-section calculations for ion-molecule collision systems. Our focus is proton impact on methane molecules (CH_4) and the five DNA and RNA nucleobases adenine ($C_5H_5N_5$), cytosine ($C_4H_5N_3O$), guanine ($C_5H_5N_5O$), thymine ($C_5H_6N_2O_2$), and uracil ($C_4H_4N_2O_2$), for which some experimental data and previous theoretical results, mostly obtained within the CNDO approach, are available for comparison. We also present CNDO results based on our own first-principles atomic cross-section calculations and demonstrate that they disagree with the IAM-PCM predictions in regions in which overlap effects are strong. The discrepancies are most pronounced for electron capture at relatively low impact energies where the projectile speed is similar to or smaller than the average orbital speed of the molecular valence electrons. We call for experimental efforts to validate (or refute) the IAM-PCM predictions for the nucleobases.

The paper is organized as follows. We briefly summarize the IAM-PCM and contrast it with the CNDO approach in Sect. 2. More details on the IAM-PCM and comparisons with the somewhat similar screening-corrected additivity rule of Ref. [15] can be found in our previous publications [20,21,23]. Results are presented in Sect. 3. We start with a look at net ionization and capture in the proton-methane collision system to illustrate a few general trends and then discuss our results for proton collisions with the DNA/RNA nucleobases. The paper ends with a few concluding remarks in Sect. 4. Atomic units, characterized by $\hbar = m_e = e = 4\pi\epsilon_0 = 1$, are used unless otherwise stated.

2 Theoretical models

The IAM-PCM amounts to representing a net cross section for a molecular target at projectile energy E and for process x, where x stands for capture ($x = \mathrm{cap}$) or ionization ($x = \mathrm{ion}$), as a weighted sum of atomic cross sections

$$\sigma^{\mathrm{net}\,x}_{\mathrm{IAM-PCM}}(E,\alpha,\beta,\gamma) = \sum_{j=1}^{N} s_j^x(E,\alpha,\beta,\gamma)\sigma_j^{\mathrm{net}\,x}(E) \quad (1)$$

with weight factors $0 \le s_j^x \le 1$ for the N atoms that make up the molecule, and the Euler angles α, β, γ which characterize the orientation of the molecule relative to the projectile beam axis.

The atomic cross sections are calculated in a DFT-inspired framework in the semiclassical approximation with straight-line projectile trajectories [22]. The initially occupied AOs are propagated in a mean-field potential composed of a (time-dependent) Coulombic projectile potential and an atomic target ground-state potential at the exchange-only level of DFT, i.e., correlation and time-dependent screening and exchange effects are neglected. The propagation is carried out using the coupled-channel two-center basis generator method (TC-BGM) [24] and the net cross sections for ionization and capture are obtained by summation of the corresponding orbital-specific transition probabilities and integration over the impact-parameter plane. This procedure has been shown to yield fairly accurate results over the impact energy range considered in this work (see, e.g., Ref. [21] and references therein).

The weights in Eq. (1) are obtained by picturing the atomic cross sections as circular disks around the equilibrium nuclear positions in the molecule and with radii $r_j(E) = [\sigma_j^{\mathrm{net}\,x}(E)/\pi]^{1/2}$ in a plane perpendicular to the ion beam axis. The combined area of overlapping circles that is "visible" to the impinging projectile is interpreted as the molecular cross section and computed by a pixel counting method [21]. The procedure is carried out for a large number of Euler angle triples to obtain an orientation-averaged cross section that can be compared with experimental data for randomly-oriented molecules.

Keeping in mind that the atomic cross sections are composed of AO-specific contributions we can write for the orientation average

$$\bar{\sigma}^{\mathrm{net}\,x}_{\mathrm{IAM-PCM}}(E) = \sum_j \bar{s}_j^x(E) \sum_k n_{k,j}^{\mathrm{ao}} \sigma_{k,j}^{\mathrm{ao}\,x}(E), \quad (2)$$

where the sum over k includes all AOs on the jth atom with nonzero occupation numbers $n^{\rm ao}_{k,j}$ and the $\bar{s}^x_j$ are orientation-averaged weight factors. Since the occupation numbers and the orbital-specific cross sections are the same for each atom of a certain species, Eq. (2) can be cast into the simpler form

$$\bar{\sigma}^{{\rm net}\,x}_{\rm IAM-PCM}(E) = \sum_i \eta^x_i(E)\sigma^{{\rm ao}\,x}_i(E), \qquad (3)$$

where the index i enumerates the occupied AOs of *different* atomic species only and η^x_i is a coefficient that is composed of occupation numbers and orientation-averaged weight factors. In the limiting case of zero overlap in which $\bar{s}^x_j = 1$ for all j and x one obtains

$$\sigma^{{\rm net}\,x}_{\rm IAM-AR}(E) = \sum_i n^{\rm ao}_i \sigma^{{\rm ao}\,x}_i(E), \qquad (4)$$

where $n^{\rm ao}_i$ is the *total* occupation number of the ith AO in the molecule. Note that by construction the IAM-AR result (4) represents an upper bound for the IAM-PCM cross section (3).

Let us compare these equations with the CNDO approach, which starts from the assumption that the net cross section is composed of MO-specific contributions

$$\sigma^{{\rm net}\,x}_{\rm CNDO}(E) = \sum_l n^{\rm mo}_l \sigma^{{\rm mo}\,x}_l(E) \qquad (5)$$

with occupation numbers $n^{\rm mo}_l$. In a second step the MO-specific cross sections $\sigma^{{\rm mo}\,x}_l$ are expressed as linear combinations of AO-specific cross sections. If the latter are independent of the MOs to which they contribute the CNDO net cross section can be written as

$$\sigma^{{\rm net}\,x}_{\rm CNDO}(E) = \sum_i \xi_i\, \sigma^{{\rm ao}\,x}_i(E), \qquad (6)$$

where ξ_i is the (fractional) *gross* population in the ith AO due to *all* initially occupied MOs [19] and the sum includes all AOs that are (partially) populated by at least one of the MOs. If one restricts the population analysis to the minimal atomic basis used in the expansion of the MOs, the index ranges in Eqs. (6), (4), and (3) are the same. Hence, the only difference between the CNDO approach, the IAM-AR and the IAM-PCM is the nature of the coefficients in these linear combinations of AO-specific cross sections. In the IAM-AR they are simply the atomic occupation numbers. In the CNDO approach they include molecular structure information via the Mulliken analysis, while in the IAM-PCM they depend on the impact energy and the process under study, because the atomic cross-section overlaps do.

A caveat of the foregoing analysis is that in the previously reported CNDO calculations the AO-specific cross sections are not completely independent of the MOs to which they contribute. In those works, the AO-specific calculations were carried out in some variant of the first-order Born approximation or a distorted-wave model, all of which involve the use of effective target charges in the construction of the final (continuum or bound projectile) states of interest. These effective charges were determined using *molecular* binding energies in Bohr's energy formula, thereby introducing an MO dependence into the AO-specific cross sections (see, e.g., [25,18]). By contrast, there is no room for such a choice in the coupled-channel TC-BGM and, accordingly, our own CNDO calculations, reported here, do satisfy Eq. (6).

Table 1. Atomic occupation numbers $n^{\rm ao}_i$, gross atomic populations ξ_i, and atomic binding energies ε_i (in a.u.) for CH_4 ($i = 1, \ldots, 4$) The gross populations are obtained from the information provided in Table III of [14] whch in turn is based on the Mulliken population analysis of [26]. The binding energies for atomic carbon are from the optimized effective potential calculations of [27] on which the present TC-BGM cross-section calculations are based.

	H($1s$)	C($1s$)	C($2s$)	C($2p$)
$n^{\rm ao}_i$	4	2	2	2
ξ_i	3.468	2.0	1.133	3.399
ε_i	0.5	10.353	0.750	0.431

3 Results and discussion

Before we look at the DNA/RNA nucleobases let us exemplify the different theoretical models discussed above for the proton-methane collision system as a test case. Table 1 lists the total atomic occupation numbers and the fractional gross populations obtained from a Mulliken analysis for CH_4 [26] together with the AO binding energies [27]. Given that the gross population of the most weakly bound orbital $\xi_{\rm C(2p)} = 3.399$ is significantly larger than the AO occupation number $n^{\rm ao}_{\rm C(2p)} = 2$ and ionization tends to increase with decreasing AO binding energy ε_i, one can expect the total net ionization cross section calculated within the CNDO approach to be larger than its IAM-AR counterpart.

Figure 1 shows that this is indeed the case. However, the enhancement is relatively small (approximately 10%) and insignificant for the comparison with the experimental data and the other calculations included in the figure. At impact energies $E \geq 700$ keV all data, including the IAM-AR and CNDO results, are in reasonable agreement, corroborating the previous conclusion that molecular structure effects are unimportant in this region [14]. Toward lower energies the present IAM-AR and CNDO results overestimate the data recommended by Rudd and coworkers [28], except at very low energies in the $E = 10-20$ keV range where ionization is a relatively weak process. This implies that the atomic cross-section overlaps are small in this region, and indeed, IAM-AR and IAM-PCM results appear to merge, similarly to what is observed at high energies ($E > 1$ MeV).

At intermediate energies the atomic cross sections are sufficiently large for overlap effects to be substantial. Around the maximum the IAM-PCM net ionization cross section is less than 60% of the IAM-AR value and in agreement

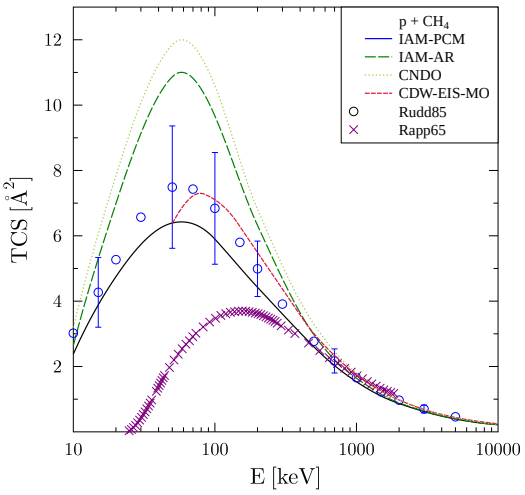

Fig. 1. Total cross section for net ionization in p-CH_4 collisions as a function of impact energy. IAM-PCM, IAM-AR, and CNDO: present calculations, CDW-EIS-MO [29]; experiments: Rudd85 [28], Rapp65 [30] for electron impact using equivelocity conversion.

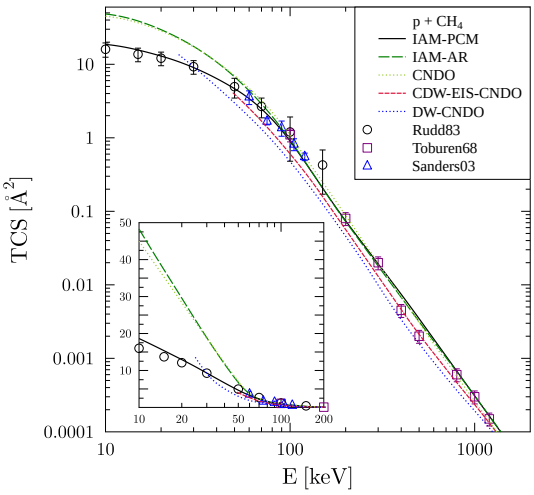

Fig. 2. Total cross section for net capture in p-CH_4 collisions as a function of impact energy. IAM-PCM, IAM-AR, and CNDO: present calculations, CDW-EIS-CNDO [18], DW-CNDO [31]; experiments: Rudd83 [32], Toburen68 [33], Sanders03 [34].

with the recommended data within the reported uncertainties. A continuum distorted-wave eikonal initial-state (CDW-EIS) calculation in which instead of the IAM or the CNDO approach a spherical-basis representation of the initial-state MOs was used [29] also agrees with the data, but results in somewhat larger cross-section values than the IAM-PCM and shows a different energy dependence with the maximum shifted toward higher energies. The latter might at least in part be due to the limited validity of the perturbative CDW-EIS model at impact energies $E < 100$ keV where electron capture gains importance as a competing reaction channel.

We have also included (absolute) electron impact measurements from [30] in Fig. 1 using equivelocity conversion. These measurements agree very well with the recommended data for proton impact above $E = 500$ keV, i.e., at projectile speeds $v \geq 4.47$ a.u. or charge-magnitude-to-speed ratios $\eta = 1/v \leq 0.22$ a.u. One can infer from this agreement that first-order perturbation theory in which cross sections do not depend on the sign of the projectile charge is valid in this region. Toward lower energies, higher-order contributions become important, as do projectile mass and, for electron projectiles, exchange effects, all of which contribute to the differences in the electron- vs. proton-impact cross sections. In particular, the electron data show a sharp threshold at the projectile speed which corresponds to the first ionization potential of CH_4 and a maximum that is shifted toward higher speeds compared to proton impact. It is interesting to see how the CDW-EIS-MO calculation of Ref. [29] appears to be able to capture the higher-order contributions quite well and agrees with the (proton-impact) measurements down to energies which correspond to η-values between 0.5 and 0.6.

Figure 2 shows results for net capture using both double- and single-logarithmic scales to emphasize different impact energy regions. The present IAM-AR and CNDO calculations yield very similar results at all energies and agree nicely with the experimental data at $E \geq 50$ keV. The close proximity of both calculations indicates that, unlike ionization, capture does not simply increase with decreasing binding energy and more than one initially occupied AO may contribute significantly. The details of the calculations show that at low impact energies the resonant capture from H($1s$) dominates, while capture from the carbon AOs gains relative importance toward higher energies. The differences in the orbital-specific cross sections and those between the gross populations and occupation numbers listed in Table 1 balance out and result in very similar IAM-AR and CNDO cross sections.

Figure 2 also includes two previous CNDO calculations; the calculation by Quinto and co-workers [18] uses the CDW-EIS model and the one by Purkait *et al.* [31] a different distorted-wave (DW) approach to calculate the AO-specific cross-section contributions. Both works yield somewhat smaller cross-section values than the present CNDO calculation, but show a similar impact energy dependence, at least down to $E = 50$ keV where the CDW-EIS calculation terminates. The cross-section curve from [31] extends further down to $E = 25$ keV and indicates an even stronger increase toward low energies than the present CNDO calculation, which significantly overestimates the measurements in this region. We note that Purkait *et al.*

also reported IAM-AR calculations in their work which for p-CH_4 collisions are in close agreement with their CNDO results. Similarly, an earlier publication of the Argentinian group reported very similar CDW-EIS IAM-AR and CNDO capture cross sections for a number of molecules, including CH_4 [25], confirming our present finding regarding the comparison of both descriptions. This suggests that the choice of *molecular* binding energies in the construction of the final states in the perturbative models has but a very small influence on the magnitude of the total capture cross section.

The present IAM-PCM results agree with the IAM-AR and CNDO calculations at high energies. They begin to deviate from the latter at $E \approx 70$ keV and follow the experimental data closely down to $E = 10$ keV where the IAM-AR capture cross section is more than twice as large. This is similar to what was found for other collision systems such as p-CO and p-H_2O [20] and gives us confidence in the validity of the IAM-PCM. The key to its success from low- to high-velocity collisions is the impact-energy dependence of the weight factors in Eq. (3). By contrast, the applicability of methods with energy-*independent* weights such as the IAM-AR and the CNDO approach appears to be more limited.

We now turn to the DNA/RNA nucleobases adenine, cytosine, guanine, thymine, and uracil. Since the observations and conclusions are very similar for all five targets, we restrict the graphical discussion and comparison with previous results to the proton-adenine collision system and provide our IAM-PCM results for the other target molecules in tabular form only. The molecular geometry information required for these calculations is taken from data available through the Molview project [35].

Experimental data for proton impact are rather scarce. For this reason, we include the recent electron-impact ionization measurements of Ref. [36] in the discussion. We do not compare the present results with the (proton-impact) cross sections obtained from a previous model calculation which combines the classical-trajectory Monte Carlo (CTMC) method with the classical over barrier model (COB) [37] to avoid overburdening the figures. The reader is referred to Refs. [38,17] for comparisons of the CTMC-COB results with perturbative CNDO calculations and the measurements for proton impact. We also note that a number of simpler (analytical) cross-section models have been proposed and applied to biomolecular targets. A discussion and some comparisons (for proton-pyrimidine collisions) were provided in Ref. [23] and are not repeated here.

Figure 3 shows the net ionization cross section for adenine target molecules. We note that this cross section was measured by Tabet *et al.* at $E = 80$ keV [39], but the data point is so high (at 155 Å^2) that it is outside the scale of the figure. The only other measurements for proton impact were reported by Iriki *et al.* [40,41]. Their data are included in Fig. 3 and appear to be somewhat lower than the electron-impact measurements of [36]. If we multiply the latter by a factor of 0.75 they almost perfectly match the proton data point at $E = 1$ MeV, which is well described by most of the theoretical calculations included in the figure. Toward lower E, the renormalized electron-impact data agree very well with the present IAM-PCM calculations in the energy range in which one would expect the proton- and electron-impact ionization cross section to be indistinguishable or very nearly so.

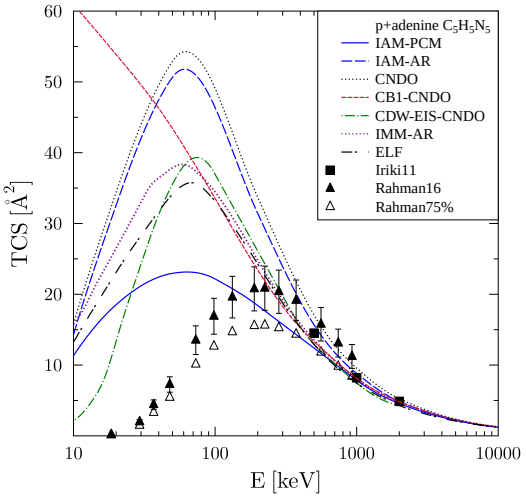

Fig. 3. Total cross section for net ionization in p-adenine ($C_5H_5N_5$) collisions as a function of impact energy. IAM-PCM, IAM-AR, and CNDO: present calculations, CB1-CNDO and CDW-EIS-CNDO [38], IMM-AR [42], ELF [43]; experiments: Iriki11 [40,41], Rahman16 [36] for electron impact using equivelocity conversion, Rahman75% are the data of [36] multiplied by 0.75.

By contrast, all other calculations predict a larger cross section below $E \approx 500$ keV. Similarly to the proton-methane case the present IAM-AR results are slightly below the CNDO and overestimate the IAM-PCM cross-section values significantly (by more than a factor of two around the maximum). Some indirect confirmation that the overlaps incorporated into the IAM-PCM mimic molecular effects appropriately comes from the independent-molecule-model (IMM) AR results included in Fig. 3. In this model, experimental cross sections for small molecules are used to assemble the cross section for the larger molecule of interest [42]. The results for adenine lie in between the IAM-PCM and IAM-AR cross sections suggesting that one can view the IMM-AR as capturing overlap effects partially, i.e., within the small molecules used to assemble the adenine ionization cross section, while overlaps between those small-molecule cross sections are not accounted for.

It is interesting to see that the IMM-AR cross-section curve is somewhat similar to the result of a semiempirical model based on the dielectric formalism whose key quantity is the so-called energy-loss function (ELF) of the target [43,44]. The cross section derived from the modelled ELF peaks at slightly higher impact energies E than its

IMM-AR counterpart and is overall smaller, but still approximately 50% larger than the IAM-PCM cross section around the maximum. The differences in height notwithstanding, most calculations agree on the position of the maximum (within $\Delta E \approx \pm 10$ keV), which, similarly to the proton-methane case shown in figure 1, occurs at significantly lower E than in the electron-impact data. New experimental data for proton-adenine collisions (and for the other nucleobases for which the situation is similar) to confirm the position of the maximum and determine the magnitude of the cross section would be highly desirable.

The present CNDO calculations are based on the Mulliken populations provided in Ref. [38], which were also used for the CDW-EIS and the first-Born with corrected boundary conditions (CB1) calculations reported in the same paper and included in Fig. 3. The two perturbative calculations are in reasonable agreement with each other down to $E \approx 70$ keV where the CDW-EIS cross section assumes its maximum, while the CB1 cross section keeps increasing toward lower energies. Both methods predict significantly smaller cross-section values than the present CNDO calculations in most of the impact energy interval shown in Fig. 3. This may be due to (i) the perturbative frameworks used in the CDW-EIS and CB1 methods vs. the nonperturbative nature of the TC-BGM, (ii) the fact that in the perturbative CNDO calculations the AO-specific cross sections include some molecular information through the choice of the final states, while the present calculations do not. Given the analysis of net capture in p-CH_4 collisions presented above the latter is unlikely, but it would be interesting to see a CDW-EIS or CB1 calculation which uses atomic instead of molecular energies for the determination of the final (continuum) states to settle this issue.

Results for net capture are shown in Fig. 4. We compare the present CNDO, IAM-AR and IAM-PCM data with the CDW and CDW-EIS CNDO calculations of Ref. [17] and the only reported experimental data point at $E = 80$ keV [39]. The CDW-EIS model produces lower cross-section values than the present CNDO calculation at all impact energies except around $E = 10$ keV which is probably outside the region of validity of the perturbative model. By contrast, the CDW model, which differs from the CDW-EIS in the choice of the distortion factor in the initial state, results in much larger cross-section values which merge with the other theoretical results only at energies $E \geq 500$ keV.

As for p-CH_4 collisions, the IAM-AR is in good agreement with the present CNDO results over most of the energy range shown. Only below $E \approx 40$ keV do the results of both models deviate somewhat more strongly than for methane. This is not surprising given the larger number of contributing electron subshells in adenine, which makes it less likely that the differences in orbital-specific capture cross sections and gross populations vs. atomic occupation numbers balance out.

The experimental data point of [39] at $E = 80$ keV is higher than all theoretical results included in Fig. 4.

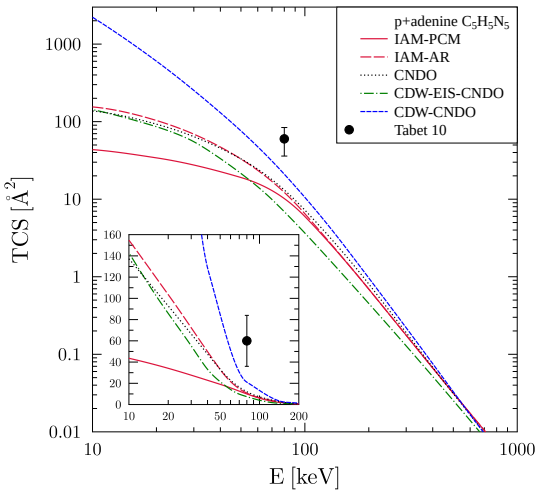

Fig. 4. Total cross section for net capture in p-adenine ($C_5H_5N_5$) collisions as a function of impact energy. IAM-PCM, IAM-AR, and CNDO: present calculations, CDW-EIS-CNDO and CDW-CNDO [17]; experiment: Tabet10 [39].

The discrepancy with the CDW CNDO calculation is perhaps acceptable, but this may be fortuitous given that the CDW model is sometimes considered inferior to the CDW-EIS because of its use of non-normalized initial-state wave functions [45]. The authors of Ref. [17] deemed the seemingly good performance of the CDW model "unexpected" and concluded that new measurements would be welcome. The present calculations reinforce the latter point. In particular, it would be of great interest if new measurements were extended to lower impact energies where the IAM-PCM predicts a much smaller capture cross section than all other theoretical models. Given the good agreement of the IAM-PCM net capture with experimental data for smaller molecules such as CH_4 (cf. Fig. 2) it would be surprising if the prediction for proton-adenine collisions would be off.

We have checked that the situation is similar for the other DNA/RNA nucleobases. In fact, all the features seen in Figs. 3 and 4 for adenine are also present for cytosine, guanine, thymine and uracil. This can be explained by the similar atomic building blocks and structures of these molecules. In lieu of figures we provide tables with the present IAM-PCM results: Table 2 lists the net capture and ionization cross sections for the pyrimidines cytosine, thymine, and uracil and Table 3 the results for the purines adenine and guanine. We note that the ionization cross sections were previously included in tables presented in [23], in which scaling properties were studied for larger classes of systems. We repeat these data here for the convenience of the reader.

Table 2. Orientation-averaged IAM-PCM net capture and ionization cross sections for proton collisions with the pyrimidines cytosine, thymine, and uracil (in Å^2).

	Cytosine ($C_4H_5N_3O$)		Thymine ($C_5H_6N_2O_2$)		Uracil ($C_4H_4N_2O_2$)	
E [keV]	Capture	Ionization	Capture	Ionization	Capture	Ionization
10	37.71	9.34	41.03	10.62	35.80	8.92
20	29.32	15.42	32.28	17.41	27.74	14.83
50	15.95	19.44	18.00	21.93	15.44	18.90
100	4.99	18.75	5.58	21.17	4.94	18.23
200	0.61	15.49	0.69	17.63	0.65	15.13
500	0.029	10.28	0.031	11.72	0.028	9.99
1000	0.0026	6.46	0.0029	7.35	0.0026	6.21
2000		3.76		4.26		3.65
5000		1.80		2.03		1.76
10000		1.02		1.14		0.98

Table 3. Orientation-averaged IAM-PCM net capture and ionization cross sections for proton collisions with the purines adenine and guanine (in Å^2).

	Adenine ($C_5H_5N_5$)		Guanine ($C_5H_5N_5O$)	
E [keV]	Capture	Ionization	Capture	Ionization
10	43.59	11.32	45.12	12.04
20	34.12	18.53	35.58	19.70
50	19.04	22.96	20.50	24.52
100	5.98	22.17	6.79	23.68
200	0.69	18.41	0.82	19.91
500	0.032	12.40	0.036	13.33
1000	0.0033	7.86	0.0036	8.47
2000		4.58		4.96
5000		2.18		2.39
10000		1.23		1.33

4 Conclusions

We have presented IAM-PCM calculations for proton collisions with methane molecules and the nucleobases adenine, cytosine, guanine, thymine, and uracil over wide ranges of impact energy from $E = 10$ keV to $E = 1$ MeV for net capture and up to $E = 10$ MeV for net ionization. Like the simpler IAM-AR and the widely-used CNDO approach the IAM-PCM is based on atomic cross-section calculations, but in contrast to the former it weighs the atomic contributions in an impact-energy-dependent way. The weight factors are obtained from the geometrical overlaps which arise when one pictures the atomic cross sections as circular disks in the impact-parameter plane. The overlaps can be substantial thereby leading to a significant reduction of IAM-PCM compared to IAM-AR cross sections. This effect is most pronounced for electron capture at low energies where we found discrepancies between IAM-PCM and IAM-AR cross sections of up to a factor of three to four. We have shown these discrepancies for proton-adenine collisions only, but have checked that they are similar for the other nucleobases. New measurements are required to test these predictions.

In the case of ionization the discrepancies between different theoretical models are less dramatic, but they are sizable, especially around the cross-section maximum. Again, these trends are similar for all nucleobases and an experimental study that would test this similarity in a systematic way would be of great interest. As for capture, the only existing experimental data points in this region appear to be too high.

In contrast to the IAM-PCM, the CNDO approach, when coupled with the present (nonperturbative) atomic-orbital-specific cross-section calculations, does not lead to significant differences to the simple IAM-AR. Previous (perturbative) work provided some evidence that the differences between both models become more pronounced when differential cross sections are calculated [14]. In the context of the present analysis it would be interesting to know if the deviations in the differential cross-section results are related to the use of molecular instead of atomic binding energies in the determination of the final continuum states in the perturbative CNDO calculations. On the level of total cross sections this choice appears to be of minor importance.

The idea to represent a molecular cross section as a combined area of overlapping atomic cross sections is not specific to proton collisions. Indeed, it would be of some interest to apply the IAM-PCM to the problem of electron-impact ionization of biomolecules, which would require accurate electron-atom ionization cross sections for all contributing atoms as input. Our own future work will focus on IAM-PCM studies of collisions involving multiply-charged projectile ions. Preliminary calculations show, not surprisingly, that the overlap effect is stronger and IAM-PCM total cross sections merge with IAM-AR results at higher impact energies than for proton impact. The role of multi-electron processes will be enhanced as well. These processes require an extension of the model to allow for the calculation of impact-parameter-dependent probabilities which can be fed into a multinomial analysis of multiple capture and ionization processes. Work in this direction is in progress.

This work was supported by the Natural Sciences and Engineering Research Council of Canada (NSERC). One of us (H. J. L.) would like to thank the Center for Scientific

Computing, University of Frankfurt for making their High Performance Computing facilities available.

Author contribution statement

All authors were involved in the reported research and the preparation of the manuscript. All authors have read and approved the final manuscript.

References

1. G. Garcia Gómez-Tejedor and M. C. Fuss, editors. *Radiation Damage in Biomolecular Systems*. Springer, Dordrecht, 2012.
2. A. V. Solov'yov, editor. *Nanoscale Insights into Ion-Beam Cancer Therapy*. Springer International Publishing, Cham, 2017.
3. B. Boudaïffa, P. Cloutier, D. Hunting, M. A. Huels, and L. Sanche. *Science*, 287:1658, 2000.
4. L. Sanche. *Eur. Phys. J. D*, 35:367, 2005.
5. C. Champion, M. E. Galassi, P. F. Weck, O. A. Fojón, J. Hanssen, and R. D. Rivarola. In G. Garcia Gómez-Tejedor and M. C. Fuss, editors, *Radiation Damage in Biomolecular Systems*, page 263. Springer, Dordrecht, 2012.
6. E. Surdutovich and A. V. Solov'yov. *Eur. Phys. J. D*, 68:353, 2014.
7. A. Verkhovtsev, E. Surdutovich, and A. V. Solov'yov. *Scientific Reports*, 6:27654, 2016.
8. M. C. Bacchus-Montabonel. *Chem. Phys. Lett.*, 664:173, 2016.
9. C. Covington, K. Hartig, A. Russakoff, R. Kulpins, and K. Varga. *Phys. Rev. A*, 95:052701, 2017.
10. E. S. Teixeira, K. Uppulury, A. J. Privett, C. Stopera, P. M. McLaurin, and J. A. Morales. *Cancers*, 10:136, 2018.
11. A. B. Salo, A. Alberg-Fløjborg, and I. A. Solov'yov. *Phys. Rev. A*, 98:012702, 2018.
12. W. H. Bragg and R. Kleeman. *Phil. Mag.*, 10:318, 1905.
13. J. W. Otvos and D. P. Stevenson. *J. Am. Chem. Soc.*, 78:546, 1956.
14. M. E. Galassi, R. D. Rivarola, M. Beuve, G. H. Olivera, and P. D. Fainstein. *Phys. Rev. A*, 62:022701, 2000.
15. F. Blanco and G. García. *Phys. Lett. A*, 317:458, 2003.
16. H. Deutsch, K. Becker, S. Matt, and T. D. Märk. *Int. J. Mass Spectrom.*, 197:37, 2000.
17. C. Champion, P. F. Weck, H. Lekadir, M. E. Galassi, O. A. Fojón, P. Abufager, R. D. Rivarola, and J. Hanssen. *Phys. Med. Biol.*, 57:3039, 2012.
18. M. A. Quinto, P. R. Montenegro, J. M. Monti, O. A. Fojón, and R. D. Rivarola. *J. Phys. B*, 51:165201, 2018.
19. R. S. Mulliken. *J. Chem. Phys.*, 23:1833, 1955.
20. H. J. Lüdde, A. Achenbach, T. Kalkbrenner, H.-C. Jankowiak, and T. Kirchner. *Eur. Phys. J. D*, 70:82, 2016.
21. H. J. Lüdde, M. Horbatsch, and T. Kirchner. *Eur. Phys. J. B*, 91:99, 2018.
22. T. Kirchner, L. Gulyás, H. J. Lüdde, E. Engel, and R. M. Dreizler. *Phys. Rev. A*, 58:2063, 1998.
23. H. J. Lüdde, M. Horbatsch, and T. Kirchner. *J. Phys. B*, 52:195203, 2019.
24. M. Zapukhlyak, T. Kirchner, H. J. Lüdde, S. Knoop, R. Morgenstern, and R. Hoekstra. *J. Phys. B*, 38(14):2353, 2005.
25. M. E. Galassi, P. N. Abufager, P. D. Fainstein, and R. D. Rivarola. *Phys. Rev. A*, 81:062713, 2010.
26. R. Hoffmann. *J. Chem. Phys.*, 39:1397, 1963.
27. K. Aashamer, T. M. Luke, and J. D. Talman. *At. Data Nucl. Data Tables*, 22:443, 1978.
28. M. E. Rudd, Y. K. Kim, D. H. Madison, and J. W. Gallagher. *Rev. Mod. Phys.*, 57:965, 1985.
29. L. Gulyás, I. Tóth, and L. Nagy. *J. Phys. B*, 46:075201, 2013.
30. D. Rapp and P. Englander-Golden. *J. Chem. Phys.*, 43:1464, 1965.
31. K. Purkait, S. Samaddar, S. Halder, C. R. Mandal, and M. Purkait. *Braz. J. Phys.*, 49:473, 2019.
32. M. E. Rudd, R. D. DuBois, L. H. Toburen, C. A. Ratcliffe, and T. V. Goffe. *Phys. Rev. A*, 28:3244, 1983.
33. L. H. Toburen, M. Y. Nakai, and R. A. Langley. *Phys. Rev.*, 171:114, 1968.
34. J. M. Sanders, S. L. Varghese, C. H. Fleming, and G. A. Soosai. *J. Phys. B*, 36:3835, 2003.
35. MolView: http://molview.org [Online; accessed 2019-13-07].
36. M. A. Rahman and E. Krishnakumar. *J. Chem. Phys.*, 144:161102, 2016.
37. H. Lekadir, I. Abbas, C. Champion, O. Fojón, R. D. Rivarola, and J. Hanssen. *Phys. Rev. A*, 79:062710, 2009.
38. M. E. Galassi, C. Champion, P. F. Weck, R. D. Rivarola, O. A. Fojón, and J. Hanssen. *Phys. Med. Biol.*, 57:2081, 2012.
39. J. Tabet, S. Eden, S. Feil, H. Abdoul-Carime, B. Farizon, M. Farizon, S. Ouaskit, and T. D. Märk. *Phys. Rev. A*, 82:022703, 2010.
40. Y. Iriki, Kikuchi Y., M. Imai, and Itoh A. *Phys. Rev. A*, 84:032704, 2011.
41. Y. Iriki, Kikuchi Y., M. Imai, and Itoh A. *Phys. Rev. A*, 84:052719, 2011.
42. S. Paredes, C. Illescas, and L. Méndez. *Eur. Phys. J. D*, 69:178, 2015.
43. P. de Vera, R. Garcia-Molina, I. Abril, and A. V. Solov'yov. *Phys. Rev. Lett.*, 110:148104, 2013.
44. P. de Vera, I. Abril, R. Garcia-Molina, and A. V. Solov'yov. *J. Phys. Conf. Series*, 438:012015, 2013.
45. L. Gulyás, A. Igarashi, and T. Kirchner. *J. Phys. B*, 45:085205, 2012.